

Stylus ion trap for enhanced access and sensing

Robert Maiwald^{1,2*}, Dietrich Leibfried³, Joe Britton³, James C. Bergquist³, Gerd Leuchs^{1,2}
and David J. Wineland³

Small, controllable, highly accessible quantum systems can serve as probes at the single-quantum level to study a number of physical effects, for example in quantum optics or for electric- and magnetic-field sensing. The applicability of trapped atomic ions as probes is highly dependent on the measurement situation at hand and thus calls for specialized traps. Previous approaches for ion traps with enhanced optical access included traps consisting of a single ring electrode^{1,2} or two opposing endcap electrodes^{2,3}. Other possibilities are planar trap geometries, which have been investigated for Penning traps^{4,5} and radiofrequency trap arrays^{6–8}. By not having the electrodes lie in a common plane, the optical access can be substantially increased. Here, we report the fabrication and experimental characterization of a novel radiofrequency ion trap geometry. It has a relatively simple structure and provides largely unrestricted optical and physical access to the ion, of up to 96% of the total 4π solid angle in one of the three traps tested. The trap might find applications in quantum optics and field sensing. As a force sensor, we estimate sensitivity to forces smaller than $1 \text{ nN Hz}^{-1/2}$.

The basic electrode geometry is shown in Fig. 1 and is formed by two concentric cylinders over a ground plane. The design provides straightforward indexing and assembly of the trap electrodes, with large solid angle access to the ion. Four extra electrodes were placed on a circle between the grounded plane and the radiofrequency electrode to break the rotational symmetry of the radiofrequency pseudopotential about the vertical axis and to compensate for stray electric fields to minimize ion radiofrequency micromotion in the trap⁹.

Three different traps were built adjacent to each other on the same test set-up (Fig. 2). These traps range from a conservative design with a larger trap depth, higher motional frequencies and a smaller accessible solid angle, to a weaker trap with greater optical access. This change in properties is achieved by varying the protrusion height Δh of the central grounded electrode with respect to the radiofrequency electrode (Table 1).

The degeneracy of motional frequencies in the radial direction was lifted by applying potentials of the order of 0.1–1 V to the compensation electrodes A–D. This created a static quadrupole field defining the principal radial axes of the trap along the lines connecting compensation electrode A with D and B with C. Thus, the axes were oriented at angles of about 45° relative to the two cooling beams (Fig. 1b). In addition, the entire trap assembly was tilted by about 7.5° with respect to the direction defined by the laser beams, ensuring that the vertical axis of the traps was not orthogonal to the wave vectors of the cooling beams. In this way, all three normal modes of the ion were sufficiently Doppler cooled by a single laser beam. For further details, see the Methods section.

To compensate radiofrequency micromotion due to electric stray fields, we varied the potential on all four compensation electrodes and the central cylinder while changing the power level of the radiofrequency drive. Compensation was achieved when the ion position remained stationary for different radiofrequency drive amplitudes⁹. We could also minimize micromotion along the direction of the cooling beam by adjusting compensation potentials and maximizing the scattering signal with the cooling beam tuned close to resonance. By lowering the radiofrequency drive after loading, we determined a minimum radiofrequency power for ‘stable’ trapping that seemed to be limited only by background gas collisions. The trap of configuration 3 was able to trap reliably after the well depth was lowered to less than 1 meV. As this depth is significantly below room temperature, ions can be lost by a single Langevin (charge-dipole) collision with a background gas atom. At the base pressure of about 3×10^{-9} Pa reached in our system, the mean ion lifetime with laser cooling was around 30 s in this particular case.

In all three traps, we observed ion lifetimes in excess of three hours under continuous laser cooling. Without cooling light, lifetimes were greater than 10 s. The secular frequencies of ion motion along all three axes were determined by applying extra sinusoidal drive potentials to the compensation electrodes or the central electrode. If the drive frequency is resonant with a secular frequency, ion motion is excited to large amplitudes, causing a sharp drop of laser-induced fluorescence.

Operating parameters for each of the three traps are summarized in Table 1 together with observed trap frequencies, radiofrequency drive voltage and trap depth as inferred from measured trap frequencies and numerical simulations for each trap. The accessible solid angle ignores the compensation electrodes and outer ground plane. This seems reasonable because in future implementations, these electrodes could be made smaller and/or recessed below the radiofrequency electrode. This has not been done so far to facilitate construction of the basic electrode structure.

The compact design permits placing the trap inside a metallic parabolic mirror, which can also serve as a radiofrequency ground electrode (Fig. 3a). By moving the trap structure, an ion can be placed at the focal point of the mirror for efficient fluorescence collection. Moreover, parallel light beams directed along the mirror optical axis are focused directly onto the ion. By appropriately shaping the transverse mode pattern of the incident light^{10,11}, the field at the focus can produce a linear dipole excitation pattern aligned with the axis of symmetry of the parabolic mirror, which could lead to very efficient photon–ion coupling¹². With electrode configuration 3 and a parabolic mirror with a depth-to-focal-length ratio of 6:1 (an aspect ratio that is feasible to manufacture), the solid angle intercepted by the parabolic mirror is 81% of 4π .

¹Institute of Optics, Information and Photonics, University of Erlangen-Nuremberg, Staudtstr. 7 | B2, 91058 Erlangen, Germany, ²Max Planck Institute for the Science of Light, Günther-Scharowsky-Str. 1, Bldg. 24, 91058 Erlangen, Germany, ³Time and Frequency Division, National Institute of Standards and Technology, 325 Broadway, Boulder, Colorado 80305, USA. *e-mail: robert.maiwald@physik.uni-erlangen.de.

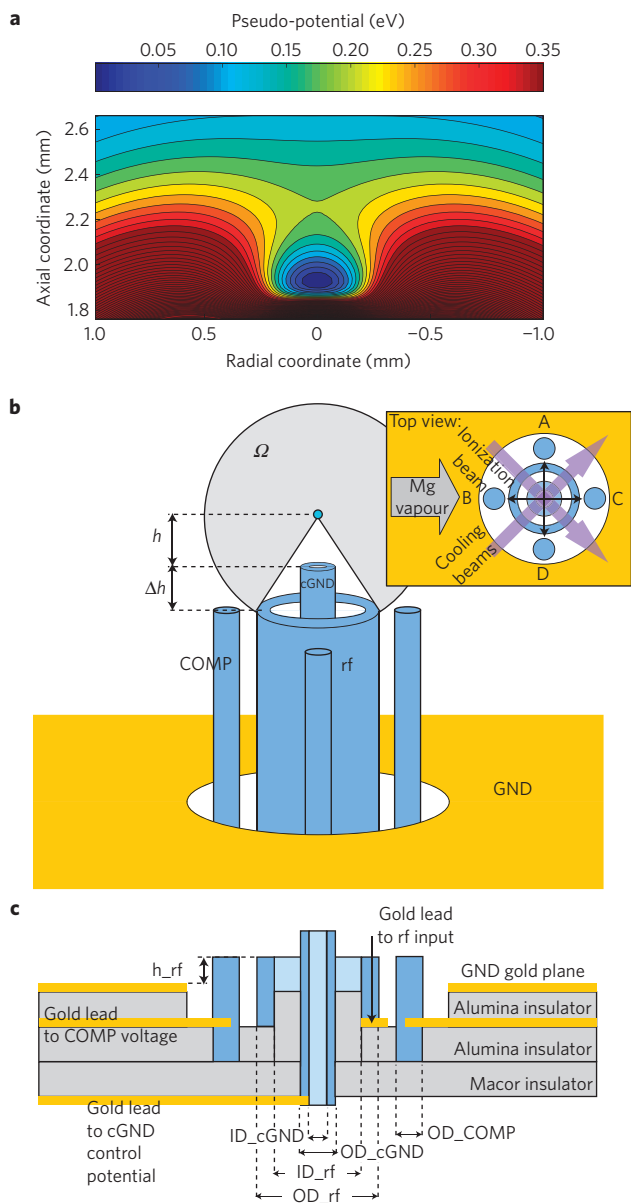


Figure 1 | Pseudo-potential and trap geometry. **a**, Simulations of the trap radiofrequency pseudopotential indicate smaller trap potential depths and binding frequencies compared with those of more traditional trap designs of similar size, radiofrequency drive frequency and amplitude. Shown is an example calculation of the pseudo-potential (in electronvolts) for electrode configuration 3 using the corresponding parameters given in Table 1 and $^{24}\text{Mg}^+$ properties, although neglecting the compensation electrodes. The isoline separation is 25 meV and the axial coordinate is measured from the grounded plane. **b**, Placement of the electrodes. The central ground electrode (cGND) is surrounded by the radiofrequency electrode (rf) and the grounded plane (GND). These electrodes provide the primary trapping potential. In addition, four symmetrically placed compensation electrodes (COMP) provide fine adjustments to the overall potential. The distance h between the ion and the centre electrode varies with Δh , the height difference between the centre electrode and the radiofrequency electrode. The accessible solid angle Ω is also illustrated. The inset shows the position of the trap electrodes with respect to the laser beams for cooling and ionization and the direction of the principal radial axes of the trap. The direction from which the neutral Mg vapour enters the trapping region is indicated. **c**, The layered assembly showing insulating planes with conducting gold leads and laser-cut holes to house the electrodes. The diagram is not drawn to scale. See the Methods section for dimensions.

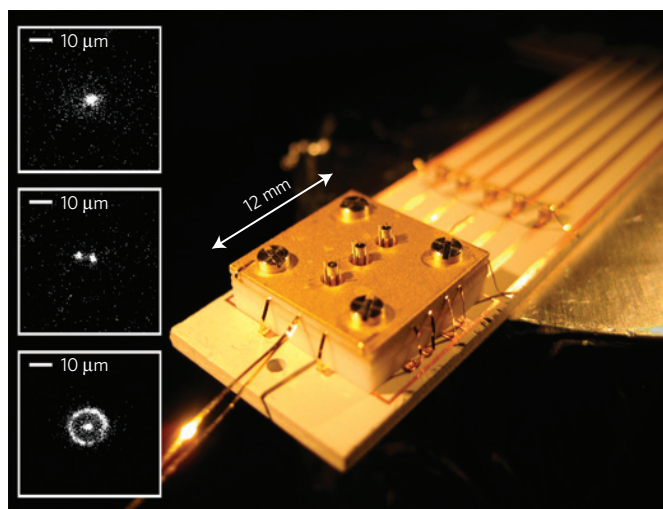


Figure 2 | The completed trap assembly before insertion into the vacuum chamber. The three test traps with differing protrusion height Δh (increasing from front to back) of the central electrode can be seen. Visible in the upper right-hand side of the figure is also the ceramic board with copper traces, which accommodates surface-mounted components constituting low-pass filters for the d.c. electrodes. Two parallel gold wires connecting the radiofrequency electrode can be seen in the lower left-hand side of the figure. The insets show different experimentally observed ion configurations (from top to bottom): a single trapped ion, two ions revealing the orientation of the weakest trap axis and an ion crystal in an approximately cylindrical potential that allows the outer ions to rotate about the trap vertical axis.

For a linear electric dipole aligned along the mirror axis, this geometry would lead to a collection efficiency of 94%. Conversely, light sent onto the ion in a dipolar pattern would provide a near-perfect atom-to-photon coupling to a linear dipole transition, possibly working down to the single-photon level^{13,14}. To this end, one could use ions with even-numbered charge that allow for $J = 0-1$ transitions¹².

This scheme might also provide a significant improvement in the efficiency of remote entanglement of trapped ions as described in refs 15–17. As an example, the entanglement scheme used in ref. 17 is based on filtering the emission of the atom on $F' = 0, 1$ to $F = 0, 1$ transitions to overlap only photons on a beam splitter resulting from π -transitions. Limitations of the experiment in ref. 17 were caused by restrictions in the collection solid angle (2% of 4π) as well as coupling of the emission pattern that was imaged through a multi-element lens into a single mode fibre (efficiency 20%). A parabolic collection mirror could potentially improve the situation because ideally it transforms the orthogonal mode patterns of photons emitted on π or σ -transitions while preserving their orthogonality¹⁸. Orthogonality is also preserved in good approximation by the remaining elements of the mode shaping proposed in refs 10, 11. Therefore, it might be possible to not only couple photons from π -transitions with near unit efficiency to a single mode fibre, but the mode converter will also act as a filter blocking out undesired photons from σ -transitions. Ideally one would expect to boost the production rate of entangled pairs by more than 5×10^4 over the values reported in ref. 17. Efficient coupling could also be obtained through a resonant interaction of an ion with a cavity^{19,20}. In this method, to achieve a coupling efficiency of 90%, a minimum cooperativity of 4.5 is required. At present, this is difficult to achieve for many ions that have ultraviolet transition wavelengths and further complications may be encountered with mirror charging^{19,20}.

Table 1 | Typical operating parameters.

Electrode configuration	Trap 1	Trap 2	Trap 3	Unit
Protrusion height Δh	0	250	500	μm
rf drive voltage U^*	290	460	400	V
rf drive frequency $\Omega_{\text{rf}}/(2\pi)$	80.15	31.94	11.85	MHz
Trap frequencies:				
—axial	1.8	2.2	2.1	MHz
—radial \overline{AD}	0.951	1.268	1.064	MHz
—radial \overline{BC}	0.907	1.233	1.007	MHz
Trap depth*	71	178	195	meV
Observed distance h	168	244	290	μm
Accessible solid angle $\Omega/(4\pi)$	71%	91%	96%	

The parameters were derived from measurements on single trapped $^{24}\text{Mg}^+$ ions. The main difference between the three traps is the protrusion height Δh of the centre electrode beyond the radiofrequency electrode (Fig. 1b). Owing to this variation, different trap frequencies and accessible solid angles are obtained. Radial \overline{AD} (\overline{BC}) indicates a normal mode direction along the line connecting compensation electrodes A and D (B and C), see also Fig. 1b. The observed distances h were 10–20% smaller than predicted by simulations. This seems reasonable because the simulations neglected the radiofrequency grounded compensation electrodes, which if included, would reduce the predicted values of h .

*These parameters are difficult to measure directly and were inferred from the measured trap frequencies and the numerical simulation of the trapping potentials.

The open geometry of such traps also suggests applications as a probe of fields near a surface. Surfaces of interest could be brought close to the ion, as in Fig. 3b. By either scanning the ion trap over the surface or translating the surface itself, one could map out the electromagnetic or force fields in proximity of the surface. Modelling the ion trap in the presence of a ground plane located horizontally above the ion in Fig. 1 indicates that a stable quadrupole minimum is retained until the distance to the surface is approximately equal to the distance of the ion to the centre electrode. In the traps described here, this would limit the ion to distances of about $170\mu\text{m}$ from the surface, a limit that could be reduced by miniaturizing the trap. The ion serves as a stylus probe tip that is extremely sensitive to forces oscillating at its motional frequencies. These frequencies can be tuned over at least two decades from approximately $\omega/(2\pi) = 100\text{ kHz}$ to 10 MHz . In addition, information on the force-field direction can be extracted by using all three non-degenerate modes of motion of the ion. With the same apparatus, static and time-dependent magnetic fields can be measured by observing first- and second-order shifts of the ion on narrow internal transitions.

To estimate the sensitivity to oscillating force fields we assume that the ion, initially cooled to its motional ground state, is driven in resonance with a motional mode for a duration $t = 1/\Delta_b$, where Δ_b is the approximate measurement bandwidth. The amplitude α of the coherent state grows as²¹

$$\alpha = \frac{Fz_0}{2\hbar}t$$

where F is the amplitude of the driving force, $z_0 = \sqrt{\hbar/(2m\omega)}$ is the size of the ion's harmonic oscillator ground-state wavefunction, m is the ion's mass and \hbar is Planck's constant divided by 2π . To yield a detectable signal, this coherent excitation has to be comparable to the excitation due to motional heating that grows according to $\langle n_n \rangle = \langle \dot{n} \rangle t$, where $\langle \dot{n} \rangle$ is the ion's heating rate^{22,23}. Heating rates in the range of $0.2\text{--}2\text{ quanta ms}^{-1}$ have been observed in traps with similar electrode-to-ion distances for a motional frequency $\omega/(2\pi) \simeq 1\text{ MHz}$ (refs 24, 25). As the geometry discussed here minimizes the amount of material close to the ion, a heating rate of one quantum per millisecond should be a realistic estimate. (For small cryogenic traps, heating rates of the order of one quantum per

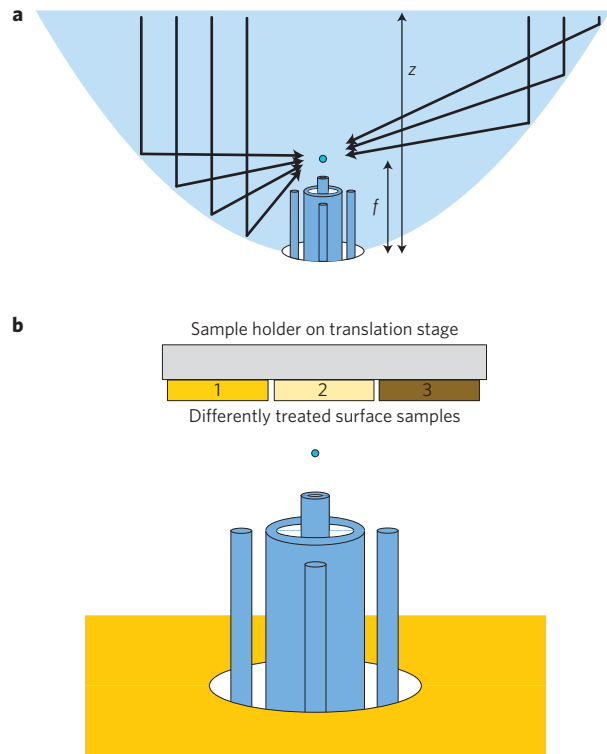


Figure 3 | Potential applications of the trap geometry. **a**, Placement of the ion in the focus f of a parabolic mirror with depth z to maximize photon-ion coupling. **b**, Scanning of different surfaces with the ion as a sensitive probe.

second have been observed²³.) Assuming a signal-to-noise ratio of one, we require $\langle n_n \rangle = \langle n_c \rangle = |\alpha|^2$ and therefore

$$\frac{F}{\sqrt{\Delta_b}} \simeq \sqrt{\langle \dot{n} \rangle} \frac{2\hbar}{z_0}$$

For $^{24}\text{Mg}^+$, $\langle \dot{n} \rangle = 1\text{ ms}^{-1}$ and $\omega/(2\pi) = 1\text{ MHz}$, this implies a force sensitivity of $0.46\text{ yN Hz}^{-1/2}$ ($1\text{ yN} = 1\text{ yocto-Newton} = 10^{-24}\text{ N}$), several orders of magnitude below the smallest forces detectable with atomic force microscopes or micromechanical cantilevers²⁶. This force sensitivity corresponds to an electric-field sensitivity of $2.9\text{ (}\mu\text{V m}^{-1}\text{) Hz}^{-1/2}$. For a cryogenic ion trap where $\langle \dot{n} \rangle = 1\text{ s}^{-1}$, the sensitivity would be increased by approximately a factor of 30.

To detect the magnetic field at the ion's position, we may excite a narrow transition (for example, a hyperfine transition) with well-known field dependence. The method would be limited by quantum projection noise²⁷. On a Zeeman-shifted transition with a magnetic moment difference of 1 Bohr magneton ($\Delta\nu/\Delta B = 14\text{ MHz mT}^{-1}$) when probed by the Ramsey method with free precession time T_R , the magnetic-field resolution ΔB is

$$\Delta B(\tau) = \frac{1}{2\pi(\Delta\nu/\Delta B)\sqrt{T_R\tau}} = 1.1 \times 10^{-11}\text{ T}/\sqrt{\tau/\text{s}}$$

where τ is the averaging time and the last expression assumes $T_R = 1\text{ s}$. By actively compensating the surface field with external coils that lead to a known field geometry, we could detect not only the modulus but also the direction of the local magnetic field. Although magnetic fields can be sensed closer to the surface using nitrogen vacancy centres^{28,29} and with higher signal-to-noise ratio with a large number of cold neutral atoms³⁰, a potential advantage of the ion sensor could be the combined sensitivity to electric and magnetic fields.

In principle, the electric field in all space can be reconstructed from the field in one plane, but this inversion is an ill-posed problem for spatial features much smaller than the ion-to-feature distance. Therefore, the lateral spatial resolution when scanning the surface will be limited by the attained signal-to-noise ratio and is roughly equal to the distance to the surface if the signal-to-noise ratio is of order one.

An interesting application of the ion sensor in quantum-information processing with trapped ions is to use it for straightforward comparisons of heating rates of different surfaces^{3,22,23}. Typically, to compare heating rates from different electrode surfaces, separate traps composed of different materials have been built and tested. This leads to uncertainties due to variations in the trap geometry, the exact steps of materials processing, surface contamination due to cleaning agents and the bake-out procedure. Most of these variables could be eliminated, and the testing of different materials could be accelerated by the use of one ion sensor on a variety of material samples deposited on the same carrier surface (Fig. 3b).

Methods

Trap fabrication and vacuum housing. The trap electrodes are made of stainless-steel rods and hypodermic tubing. The dimensions indicated in Fig. 1 are as follows: OD_rf = 710 μm , ID_rf = 535 μm , OD_cGND = 205 μm , ID_cGND = 100 μm , OD_COMP = 150 μm , h_rf = 1,110 μm . Structural integrity and insulation is provided by a combination of alumina and Macor spacers. Electrical connections were made by resistive welding of gold ribbons to the trap electrodes and to gold traces (thickness 5–10 μm) that were silk-screened onto alumina. The outer ground plane was also formed by this silk-screening process. All insulating surfaces have been recessed or positioned to prevent a direct line of sight to the ion position. This suppresses distortions of the trapping field caused by charged insulating surfaces. The potentials applied to the individual d.c. electrodes (central ground and compensation electrodes A–D) are passively filtered by resistor–capacitor low-pass filters with $R = 1 \text{ k}\Omega$ and $C = 2 \text{ nF}$. The components are mounted on a connection board inside the vacuum close to the trap.

The assembled trap package is attached to the connection board (Fig. 2), which is in turn mounted inside a copper tube that forms part of a radiofrequency resonator that supplies the radiofrequency potential. The traps, Mg ovens and copper tube reside inside a quartz envelope with extrusions and flat windows for laser beams and for imaging of the trapped ions. The vacuum system is completed by a 20 l s^{-1} ion getter pump, a Ti-sublimation pump and an ionization pressure gauge. The system was pumped to $5 \times 10^{-5} \text{ Pa}$ and baked-out at 210°C for 8 days. After cooling the system to room temperature and several applications of Ti-sublimation, a base pressure of about $3 \times 10^{-9} \text{ Pa}$ (at the gauge) was achieved.

Helical resonators were driven by a low-noise signal generator to generate the radiofrequency trap potentials. They had loaded Q -factors ranging from 300 to 430 and were driven with input powers in the range of 22 to 35 dB m. This resulted in radiofrequency amplitudes (inferred from simulations and the resulting trap frequencies) in the range of 290–460 V.

Photoionization loading, Doppler laser cooling and detection. A ^{24}Mg oven produced a vapour of neutral atoms that was directed at the traps in the horizontal direction of Fig. 1b. To load ions into the traps, the neutral atoms inside the confinement region were then photoionized. All experiments were carried out at a magnetic field of $B \approx 0 \text{ T}$. Photoionization and Doppler laser cooling were achieved by crossing three laser beams in the confinement region of a selected trap. The photoionization beam ($\lambda = 285 \text{ nm}$, 2–4 mW, 50 μm waist) was resonant with the $3s^2 \ ^1S_0 \leftrightarrow 3s3p \ ^1P_1$ transition in neutral Mg (ref. 25). A second photon either at 285 nm or at 280 nm (below) promotes the electron from the $3s3p \ ^1P_1$ state to the continuum, producing a $^{24}\text{Mg}^+$ ion in the confinement region. For cooling, a second laser beam ($\lambda = 280 \text{ nm}$, 1 mW, 30 μm waist) was tuned about 400 MHz below the $3s^2 \ ^2S_{1/2} \leftrightarrow 3s3p^2 \ ^1P_{1/2}$ transition of $^{24}\text{Mg}^+$ for initial cooling. A third, much weaker beam ($\lambda = 280 \text{ nm}$, 2–10 μW), with intensity below saturation and tuned below the $3s^2 \ ^2S_{1/2} \leftrightarrow 3s3p^2 \ ^1P_{1/2}$ transition by half of the natural linewidth ($\approx 20 \text{ MHz}$), subsequently cooled the ions to near the Doppler limit. At that point, photon scattering and cooling was dominated by the closely detuned beam. In the case of sudden ion heating, for example due to a collision with background gas, the 400 MHz detuned beam could efficiently recoil the ion to a point where the near-resonant beam would take over.

The ion was detected by collecting fluorescence with a high-numerical-aperture ($\text{NA} \approx 0.4$) objective located a distance of 5 cm above the ion, and either imaged onto an electron-multiplying charge coupled imaging device or photomultiplier tube.

Received 14 November 2008; accepted 29 May 2009;
published online 28 June 2009

References

1. Yu, N., Nagourney, W. & Dehmelt, H. Demonstration of new Paul–Straubel trap for trapping single ions. *J. Appl. Phys.* **69**, 3779–3781 (1991).
2. Schrama, C., Peik, E., Smith, W. & Walther, H. Novel miniature ion traps. *Opt. Commun.* **101**, 32–36 (1993).
3. Deslauriers, L. *et al.* Scaling and suppression of anomalous heating in ion traps. *Phys. Rev. Lett.* **97**, 103007 (2006).
4. Stahl, S. *et al.* A planar Penning trap. *Eur. Phys. J. D* **32**, 139–146 (2005).
5. Castrejoan-Pita, J. R. *et al.* Novel designs for Penning ion traps. *J. Mod. Opt.* **11**, 1581–1594 (2007).
6. Chiaverini, J. *et al.* Surface electrode architecture for ion-trap quantum information processing. *Quantum Inf. Comput.* **5**, 419–439 (2005).
7. Seidelin, S. *et al.* Microfabricated surface-electrode ion trap for scalable quantum information processing. *Phys. Rev. Lett.* **96**, 253003 (2006).
8. Pearson, C. E. *et al.* Experimental investigation of planar ion traps. *Phys. Rev. A* **73**, 032307 (2006).
9. Berkeland, D. J., Miller, J. D., Bergquist, J. C., Itano, W. M. & Wineland, D. J. Minimization of ion micromotion in a Paul trap. *J. Appl. Phys.* **83**, 5025–5033 (1998).
10. Quabis, S., Dorn, R., Eberler, M., Glöckl, O. & Leuchs, G. Focusing light to a tighter spot. *Opt. Commun.* **179**, 1–7 (2000).
11. Lindlein, N. *et al.* A new 4π geometry optimized for focusing on an atom with a dipole-like radiation pattern. *Laser Phys.* **17**, 927–934 (2007).
12. Sondermann, M. *et al.* Design of a mode converter for efficient light-atom coupling in free space. *Appl. Phys. B* **89**, 489–492 (2007).
13. Stobińska, M., Alber, G. & Leuchs, G. Perfect excitation of a matter qubit by a single photon in free space. *EPL* **86**, 14007 (2009).
14. Pinotsi, D. & Imamoglu, A. Single photon absorption by a single quantum emitter. *Phys. Rev. Lett.* **100**, 093603 (2008).
15. Moehring, D. L. *et al.* Entanglement of single-atom quantum bits at a distance. *Nature* **449**, 68–72 (2007).
16. Gerber, S. *et al.* Quantum interference from remotely trapped ions. *New J. Phys.* **11**, 013032 (2009).
17. Olmschenk, S. *et al.* Quantum teleportation between distant matter qubits. *Science* **323**, 486–489 (2009).
18. Sondermann, M., Lindlein, N. & Leuchs, G. Maximizing the electric field strength in the foci of high numerical aperture optics. Preprint at <<http://arxiv.org/abs/0811.2098>> (2008).
19. Mundt, A. B. *et al.* Coupling a single atomic quantum bit to a high finesse optical cavity. *Phys. Rev. Lett.* **89**, 103001 (2002).
20. Keller, M., Lange, B., Hayasaka, K., Lange, W. & Walther, H. Continuous generation of single photons with controlled waveform in an ion-trap cavity system. *Nature* **431**, 1075–1078 (2004).
21. Carruthers, P. & Nieto, M. M. Coherent states and the forced quantum oscillator. *Am. J. Phys.* **33**, 537–544 (1965).
22. Turchette, Q. A. *et al.* Heating of trapped ions from the quantum ground state. *Phys. Rev. A* **61**, 063418 (1999).
23. Labaziewicz, J. *et al.* Suppression of heating rates in cryogenic surface-electrode ion traps. *Phys. Rev. Lett.* **100**, 013001 (2007).
24. Deslauriers, L. *et al.* Zero-point cooling and low heating of trapped $^{111}\text{Cd}^+$ ions. *Phys. Rev. A* **70**, 043408 (2004).
25. Epstein, R. J. *et al.* Simplified motional heating rate measurements of trapped ions. *Phys. Rev. A* **76**, 033411 (2007).
26. Mamin, H. J. & Rugar, D. Sub-attoneutron force detection at millikelvin temperature. *Appl. Phys. Lett.* **79**, 3358–3360 (2001).
27. Itano, W. M. *et al.* Quantum projection noise: Population fluctuations in two-level systems. *Phys. Rev. A* **47**, 3554–3570 (1993).
28. Balasubramanian, G. *et al.* Nanoscale imaging magnetometry with diamond spins under ambient conditions. *Nature* **455**, 648–651 (2008).
29. Taylor, J. M. *et al.* High-sensitivity diamond magnetometer with nanoscale resolution. *Nature Phys.* **4**, 810–816 (2008).
30. Vengalattore, M. *et al.* High-resolution magnetometry with a spinor Bose–Einstein condensate. *Phys. Rev. Lett.* **98**, 200801 (2007).

Acknowledgements

This work was supported by IARPA and the NIST Quantum Information Program. We thank C. Ospelkaus and S. Ospelkaus for comments on the manuscript.

Author contributions

Experimental work by R.M., J.B., D.L. and J.C.B. Theoretical work by D.L., R.M., D.J.W. and G.L.

Additional information

Reprints and permissions information is available online at <http://npg.nature.com/reprintsandpermissions>. Correspondence and requests for materials should be addressed to R.M.